Probing cosmic isotropy with Gamma-ray bursts: A dipole and quadrupole analysis of BATSE and Fermi GBM data

Debosi Mondal[1,*], Biswajit Pandey[1,†], and Amit Mondal[‡]

[1] Department of Physics, Visva-Bharati University, Santiniketan, Birbhum, 731235, India

November 3, 2025

Abstract

The cosmological principle, asserting large-scale homogeneity and isotropy, underpins the standard model of cosmology. Testing its validity using independent astronomical probes remains crucial for understanding the global structure of the Universe. We investigate the angular distribution of Gamma-Ray Bursts (GRBs) using two of the most comprehensive all-sky datasets available, the BATSE (CGRO) and Fermi GBM catalog to test the isotropy of the GRB sky at large angular scales. We perform spherical harmonic decomposition of the GRB sky maps and estimate the dipole and quadrupole amplitudes. Statistical significance is evaluated by comparing the observed multipole amplitudes against distributions derived from 500 Monte Carlo realizations of isotropic skies. Our results show that the observed dipole amplitudes for both BATSE and Fermi GBM datasets lie within the 1σ region of their respective null distributions. However, the quadrupole amplitude in the raw BATSE and Fermi skies appears elevated at 3.7σ and 3.0σ respectively. After incorporating the BATSE sky exposure function, this apparent quadrupole anisotropy vanishes, indicating that instrumental non-uniformities fully account for the signal. Our method's reliability is validated through controlled simulations, which show it can detect the injected dipoles in BATSE-sized isotropic skies. These findings reinforce the statistical isotropy of the GRB sky and underscore the importance of accurate exposure corrections in cosmological anisotropy analyses.

Keywords: Gamma-ray bursts - Cosmological principle - Large-scale structure of the Universe

1 Introduction

One of the most fundamental assumption in cosmology is the cosmological principle, the notion that, when viewed on large enough scales, the Universe exhibits no preferred location or direction. This principle forms the backbone of the Friedmann-Lemaitre-Robertson-Walker (FLRW) metric, the geometry behind our standard model of cosmology. A range of observations support this framework, with one of the most compelling evidences being the high degree of uniformity observed in the cosmic microwave background (CMB), a relic radiation from the early Universe (Penzias and Wilson 1965; Smoot et al. 1992). Additional evidence for isotropy comes from various independent tracers, including the angular

*E-mail: debosimondal@gmail.com
†E-mail: biswap@visva-bharati.ac.in (Corresponding author)
‡E-mail: amitmondal.bwn95@gmail.com

distributions of gamma-ray bursts (Meegan et al. 1992), Type Ia supernovae (Gupta and Saini 2010), distant radio sources (Blake and Wall 2002), the X-ray background (Wu et al. 1999), large-scale galaxy surveys (Gibelyou and Huterer 2012; Pandey 2017; Sarkar et al. 2019; Sarkar and Pandey 2019; Franco et al. 2024), and the spatial distribution of galaxy clusters (Bengaly et al. 2017). Collectively, these observations provide broad support for the large-scale statistical isotropy of the Universe.

In recent years, several observational studies have investigated potential deviations from large-scale isotropy (Aluri et al. 2023). These include analyses of peculiar velocity flows in Type Ia supernovae (Colin et al. 2019), measurements of dipole anisotropies in the quasar distribution (Secrest et al. 2021; Secrest et al. 2022; Kothari et al. 2024), and reported hemispherical asymmetries in galaxy number counts (Wiegand et al. 2014; Appleby et al. 2022). Additionally, large-scale cosmic structures such as filaments and sheets (Sarkar et al. 2023), the Large Quasar Groups (LQGs) (Clowes et al. 2013), correlations in quasar orientations (Friday et al. 2022), and extensive underdense regions or voids (Keenan et al. 2013; Haslbauer et al. 2020) have been identified and examined for their implications on isotropy. While each of these findings is accompanied by methodological uncertainties and remains under active investigation, they collectively underscore the importance of continued and more precise testing of the cosmological principle. Should statistically significant deviations from isotropy be established, it could prompt a re-evaluation of the standard cosmological framework based on the FLRW metric.

Gamma-ray bursts (GRBs) are among the most energetic and luminous events in the Universe, releasing intense bursts of gamma radiation that can outshine entire galaxies for brief periods. They are typically classified into long and short bursts, believed to originate from different astrophysical progenitors such as collapsing massive stars and compact binary mergers (Kouveliotou et al. 1993). Due to their brightness and detectability across cosmological distances, GRBs serve as powerful tracers of the large-scale structure of the Universe, making them promising probes for testing the fundamental assumption of cosmic isotropy.

A growing body of research has investigated the isotropy of the Universe using gamma-ray bursts (GRBs), offering valuable insights into the validity of the cosmological principle. The isotropic angular distribution of GRBs was among the earliest indications of their extragalactic origin, as highlighted in the seminal work by Meegan et al. (1992), which showed that while the burst intensity distribution deviated from the expected Euclidean $-3/2$ power-law, the angular distribution remained statistically isotropic strongly disfavoring a Galactic origin. Building on this, Briggs et al. (1996) analyzed the first 1005 GRBs from BATSE using dipole and quadrupole statistics, concluding that the observed distributions were highly consistent with isotropy and far more uniform than any known Galactic population, thereby favouring a cosmological origin.

Subsequent investigations have uncovered a more nuanced picture, particularly when GRBs are split by duration or brightness. Tarnopolski (2017) applied a suite of statistical tools to the Fermi/GBM dataset and found that while long GRBs appear isotropic, short GRBs display significant anisotropies with confidence levels exceeding 99.98%. Similarly, Vavrek et al. (2008) divided the BATSE sample into short, long, and intermediate-duration subgroups and applied a number of statistical tools including Voronoi tessellation, minimal spanning tree, and multifractal analysis concluding that short and intermediate GRBs deviate significantly from randomness, while long GRBs are consistent with an isotropic sky. Complementary results were reported by Bernui et al. (2008), who used coordinate-independent angular correlation analyses of BATSE short GRBs and, after correcting for non-uniform sky exposure, found no intrinsic anisotropies, suggesting that observed deviations could arise from instrumental effects rather than cosmological ones. Further studies expanded this investigation beyond angular positions to redshift-dependent clustering. Balázs et al. (1999) identified a statistically significant quadrupole component in the BATSE sky map and suggested that the anisotropy observed particularly among short GRBs was not fully attributable to instrumental bias. Mészáros (2019) surveyed the body of work suggesting anisotropic patterns in GRB distributions and posited that the existence of giant structures traced by GRBs challenges the foundational assumptions of isotropy. Řípa and Shafieloo (2019) examined isotropy in GRB properties such as duration and fluence across several catalogs, and found broad consistency with statistical isotropy. Andrade et al. (2019) showed that position uncertainties in Fermi GBM GRBs can introduce spurious anisotropies in angular correlation functions, and once properly accounted for, the sky distribution of GRBs remains statistically isotropic even for short bursts. Balázs et al. (2018) found several ring-like spatial configurations in GRB redshift distributions, such as the Giant GRB Ring, but emphasized that such local irregularities do not justify rejecting the cosmological principle. Bagoly et al. (2022) similarly tested the spatial two-point correlation function using all known GRBs with spectroscopic redshifts and found no statistically significant large-scale clustering, apart from a marginal deviation in one sky patch. Most recently, Horvath et al. (2024) identified clustering in both Galactic hemispheres, including the Hercules-Corona Borealis Great Wall and the Giant GRB Ring, which have grown more prominent with the increasing GRB sample size. Though provocative, the interpretation of these structures remains contentious. Collectively, these studies demonstrate both the promise and the complexity of using GRBs to test cosmological isotropy, motivating the need for rigorous, simulation-based analyses to robustly assess potential deviations from the standard cosmological model.

The BATSE (Burst and Transient Source Experiment) catalog, compiled during the Compton Gamma Ray Observatory mission (1991–2000), includes 2702 GRBs with nearly full-sky coverage (Paciesas et al. 1999). The Fermi Gamma-ray Burst Monitor (GBM), operational since 2008 aboard the Fermi satellite, has detected over 4000 GRBs to date, with a broader energy range and improved temporal resolution (von Kienlin et al. 2020). These two datasets represent the most extensive all-sky samples of GRBs available, enabling robust statistical analyses across different missions and detection strategies. Their combined use not only enhances the statistical power of our study but also allows for a cross-validation of isotropy tests across independent datasets.

A non-zero dipole in the distribution of GRBs would indicate a directional anisotropy, a statistically significant excess of GRBs in one region of the sky compared to its opposite. Similarly, a non-zero quadrupole in the distribution of GRBs would indicate a planar or axial anisotropy, suggesting a systematic variation in the number of bursts across two opposite hemispheres or along a preferred plane in the sky. These would challenge the cosmological principle, which assumes the Universe is isotropic on large scales. In this study, we examine the angular isotropy of gamma-ray bursts using a statistical framework applied to two of the most comprehensive and widely used GRB datasets: the BATSE and Fermi GBM catalogs. We measure the dipoles and quadrupoles in these datasets and assess their statistical significance. While previous analyses have considered dipole patterns in GRB distributions (Briggs et al. 1996), our methodology advances this line of inquiry by generating empirical dipole amplitude distributions from Monte Carlo simulations of isotropic skies. By comparing the observed dipole amplitudes to these simulated distributions, we obtain a direct and statistically robust estimate of the significance of any detected anisotropy. To further validate the reliability of our approach, we perform control tests using mock GRB skies with injected dipole signatures, thereby ensuring that our framework is sensitive to known deviations from isotropy. This simulation-driven methodology provides a systematic and data-driven means of testing the null hypothesis of angular isotropy in GRB distributions.

The remainder of this paper is organized as follows. In Section 2, we outline the datasets used and the methodology adopted. Section 3 details the results of our analysis. Finally, Section 4 provides a summary of our findings and concluding remarks.

2 Data and Method of Analysis

2.1 GRB Catalogs

This study utilizes two of the most comprehensive GRB datasets available: the BATSE Gamma-Ray Burst Catalog and the Fermi GBM Burst Catalog. All data were accessed on June 24, 2025, from publicly available sources.

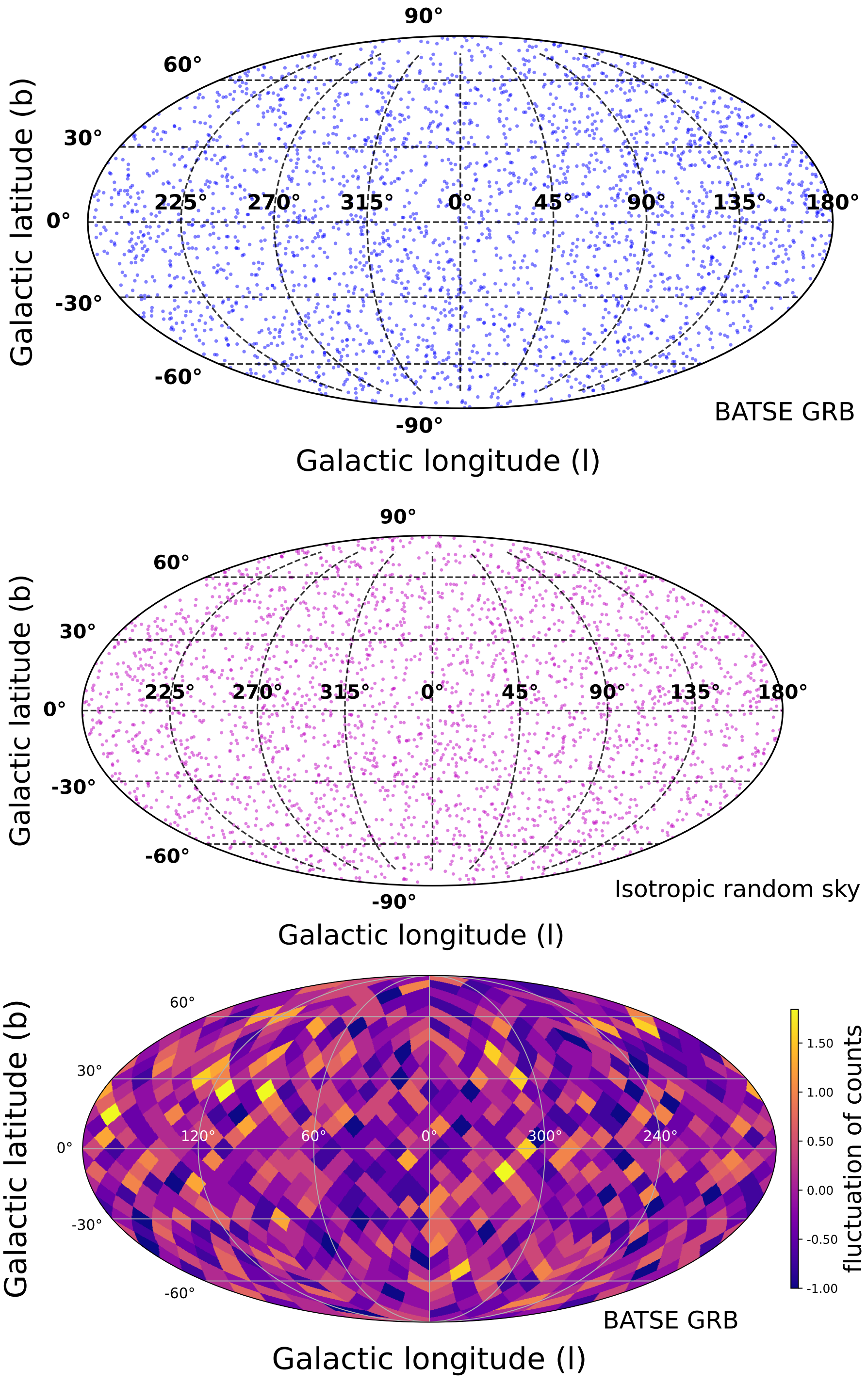

Figure 1: This shows the angular distribution of 2702 GRBs from the BATSE catalog (top panel) and a uniform random distribution of 2702 simulated points (middle panel), shown in Mollweide projection and Galactic coordinates. Bottom panel shows HEALPix map of fluctuation of GRBs from the BATSE catalog using $\mathrm{N_{side}} = 8$.

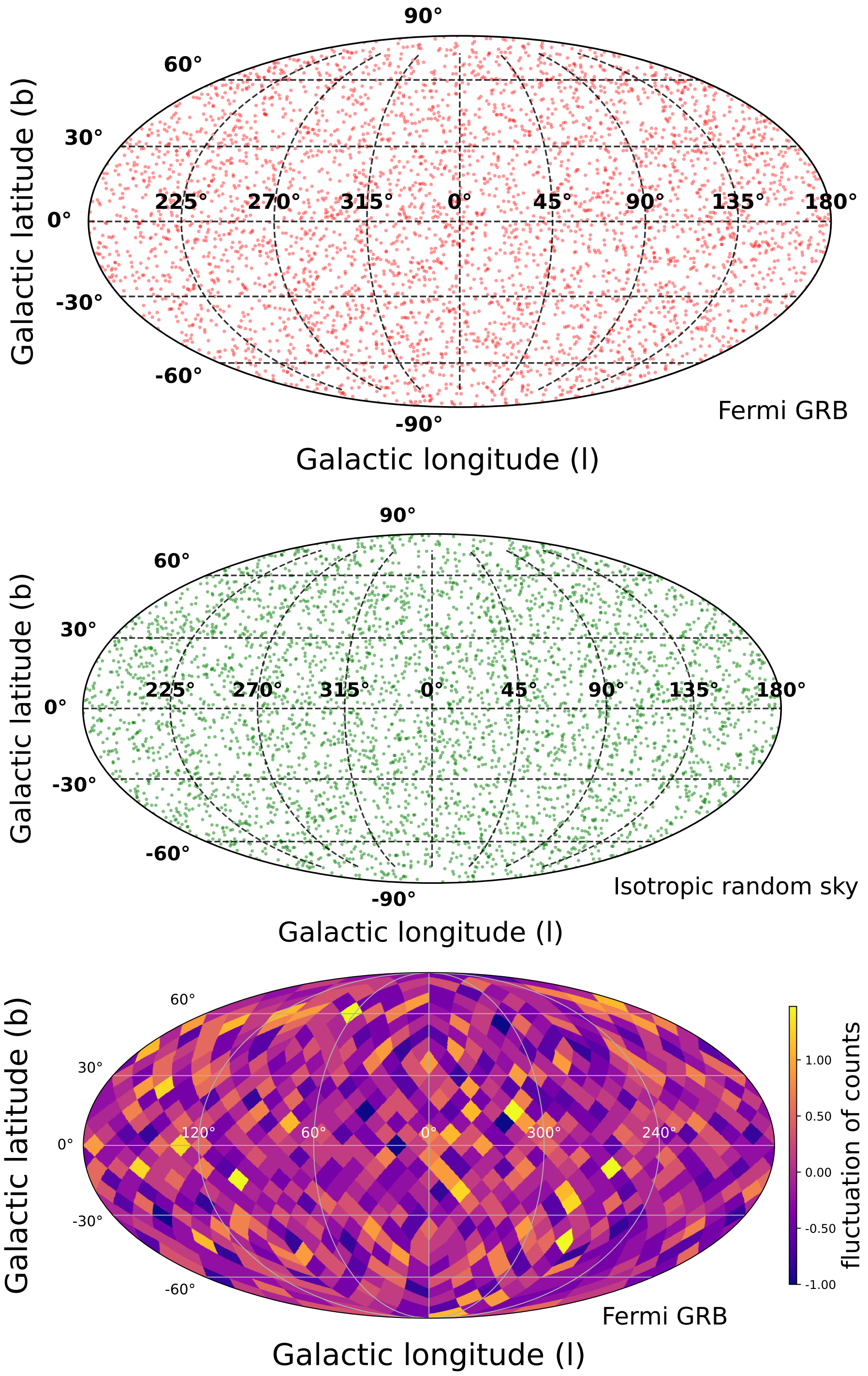

Figure 2: This shows the angular distribution of 4032 GRBs from the Fermi GBM catalog (top panel) and a uniform random distribution of 4032 simulated points (middle panel), shown in Mollweide projection and Galactic coordinates. Bottom panel shows HEALPix map of fluctuation of GRBs from the Fermi GBM catalog using $\mathrm{N_{side}} = 8$.

2.1.1 BATSE GRB catalog

Our first GRB dataset is from the *Compton Gamma Ray Observatory (CGRO)/BATSE Gamma-Ray Burst Catalog*[1] (Paciesas et al. 1999; Goldstein et al. 2013), which compiles GRBs detected by the Burst and Transient Source Experiment (BATSE) onboard CGRO between 1991 and 2000. This includes events listed in the BATSE 4B Catalog Paciesas et al. (1999), as well as additional bursts detected after its publication. The BATSE 3B Catalog Meegan et al. (1996) is also referenced as an earlier version of the dataset. A total of 2702 GRBs are included, with detection dates ranging from April 21, 1991, to May 26, 2000 (Figure 1).

2.1.2 Fermi GBM GRB catalog

Our second GRB dataset is the *Fermi GBM Burst Catalog*[2] (Goldstein et al. 2012; Paciesas et al. 2012; von Kienlin et al. 2014; Gruber et al. 2014; Narayana Bhat et al. 2016; von Kienlin et al. 2020), containing GRBs detected by the Gamma-ray Burst Monitor (GBM) onboard the Fermi Gamma-ray Space Telescope, operational since 2008. This continuously updated catalog is among the most complete and homogeneous GRB datasets to date. Our analysis includes 4032 GRBs, with detection dates spanning from July 14, 2008, to June 21, 2025 (Figure 2).

2.2 Method of Analysis

2.2.1 Sky pixelation and GRB distribution

To analyze the angular distribution of GRBs on the celestial sphere, the equatorial coordinates (RA, Dec) were first converted to Galactic coordinates (l, b), where $l \in [0°, 360°]$ and $b \in [-90°, +90°]$.

We employed the Hierarchical Equal Area isoLatitude Pixelization (HEALPix) scheme Górski et al. (2005) to divide the sky into equal-area pixels. For a given resolution parameter N_{side}, the sky is partitioned into $N_{\text{pix}} = 12 \times N_{\text{side}}^2$ pixels, each covering an area of $\frac{41253}{N_{\text{pix}}}$ deg^2. HEALPix ensures each pixel subtends the same solid angle at the center of the celestial sphere.

Using the `ang2pix` function, we obtained the number count of GRBs in each pixel and then calculated the fluctuations from the mean, resulting in a discretized distribution function $f(\theta, \phi)$, where $\theta \in [0°, 180°]$ and $\phi \in [0°, 360°]$ represent spherical polar coordinates. The fluctuations $f(\theta, \phi)$ in each pixel is defined as $\frac{n(\theta,\phi)-\bar{n}}{\bar{n}}$ where $n(\theta, \phi)$ and $\bar{n}$ are number count in (θ, ϕ) direction and mean count respectively.

2.2.2 Dipole estimation via spherical harmonics

To test for isotropy, we decomposed the GRB distribution function $f(\theta, \phi)$ into spherical harmonics $Y_{\ell m}(\theta, \phi)$, retaining terms up to the dipole level:

$$f(\theta, \phi) = \sum_{\ell=0}^{1} \sum_{m=-\ell}^{\ell} a_{\ell m} \, Y_{\ell m}(\theta, \phi)$$

Here, the monopole term ($\ell = 0$) reflects uniform distribution, while the dipole term ($\ell = 1$) captures any directional dependence. The coefficients $a_{\ell m}$ were calculated using:

$$a_{\ell m} = \int_0^{2\pi} \int_0^{\pi} f(\theta, \phi) \, Y_{\ell m}^*(\theta, \phi) \, \sin\theta \, d\theta \, d\phi$$

[1] `https://heasarc.gsfc.nasa.gov/W3Browse/cgro/batsegrb.html`
[2] `https://heasarc.gsfc.nasa.gov/W3Browse/fermi/fermigbrst.html`

The dipole amplitude is given by,

$$A_{\text{dipole}} = \sqrt{a_{1-1}^2 + a_{10}^2 + a_{11}^2}$$

We employed the dipole estimator proposed by Secrest et al. Secrest et al. (2021), implemented via the `fit_dipole` routine from the `healpy` Python package Zonca et al. (2019), which performs a linear least-squares fit of a monopole and dipole model to the HEALPix map.

2.2.3 Monte Carlo simulations and hypothesis testing

To evaluate the statistical significance of the observed dipole amplitude, we generated 500 Monte Carlo realizations of isotropically distributed skies, each containing the same number of GRBs as the respective real datasets (2702 for BATSE, 4032 for Fermi GBM). For each simulated sky, we calculated the dipole amplitude using the same methodology described above.

These simulated amplitudes were then used to construct a probability density function (PDF) for the dipole amplitude under the assumption of isotropy. The PDFs were smoothed using Kernel Density Estimation (KDE).

We then compared the dipole amplitude from the observed GRB data with the corresponding PDF to assess statistical significance. This constitutes a one-tailed hypothesis test, with the null hypothesis H_0 stating that the GRB sky is isotropic and any observed dipole arises from random fluctuations.

The significance level was set at $\alpha = 0.05$ (corresponding to a 95% confidence level). The p-value was computed as $p = P(X \geq x_{\text{obs}}) = \int_{x_{\text{obs}}}^{\infty} f(x)\,dx$. If $p < \alpha$, we reject the null hypothesis, indicating statistically significant anisotropy. Conversely, if $p \geq \alpha$, we conclude that the observed dipole amplitude is consistent with statistical fluctuations in an isotropic sky.

2.2.4 Validation with simulated dipole skies

To assess the reliability of our dipole analysis framework, we perform a controlled validation by generating simulated GRB skies with injected dipole anisotropy. These synthetic skies are constructed to contain the same number of points as the real BATSE catalog (2702 GRBs), but with a statistically imposed directional dependence. We then apply our full analysis pipeline to these mock datasets to determine whether the injected dipole signals can be recovered with statistical significance.

To simulate a GRB sky with dipole modulation, we use the following dipole-modified probability density function,

$$P(\theta, \phi) = N\left(1 + a\cos\gamma\right), \tag{1}$$

where a is the dipole strength parameter, N is a normalization constant ensuring the total probability integrates to one over the sphere, and γ is the angle between the dipole direction $(\theta_{\text{dipole}}, \phi_{\text{dipole}})$ and the point (θ, ϕ) on the sky. The angle γ is computed using the spherical law of cosines:

$$\cos\gamma = \cos\theta\cos\theta_{\text{dipole}} + \sin\theta\sin\theta_{\text{dipole}}\cos(\phi - \phi_{\text{dipole}}). \tag{2}$$

To ensure that the probability distribution remains valid, i.e., $P(\theta, \phi) > 0$, we restrict the dipole amplitude to $|a| < 1$.

We generate random (θ, ϕ) pairs uniformly over the sphere and evaluate $P(\theta, \phi)$ for each point. A (θ, ϕ) pair is accepted if a uniformly drawn random number $u \in [0, P_{\text{max}}]$ satisfies $u < P(\theta, \phi)$. Otherwise, we reject the (θ, ϕ) pair. This rejection sampling is repeated until 2702 accepted points are obtained, resulting in a simulated sky with a specified dipole anisotropy.

For our validation, we set the dipole direction to $(\theta_{\text{dipole}}, \phi_{\text{dipole}}) = (40^\circ, 140^\circ)$ and generate four dipole-injected skies with amplitudes $a = 0.09, 0.10, 0.12$, and 0.14 in Equation 1. For each realization, we compute the dipole amplitude using the same methodology as described in Section 2.2.2, and compare the results with the null distribution obtained from isotropic Monte Carlo simulations.

Figure 3 shows the dipole amplitudes of the four simulated skies superimposed on the PDF constructed from 500 isotropic sky realizations. Table 1 summarizes the corresponding p-values and their statistical significance in terms of standard deviations (σ) from the mean of the null distribution.

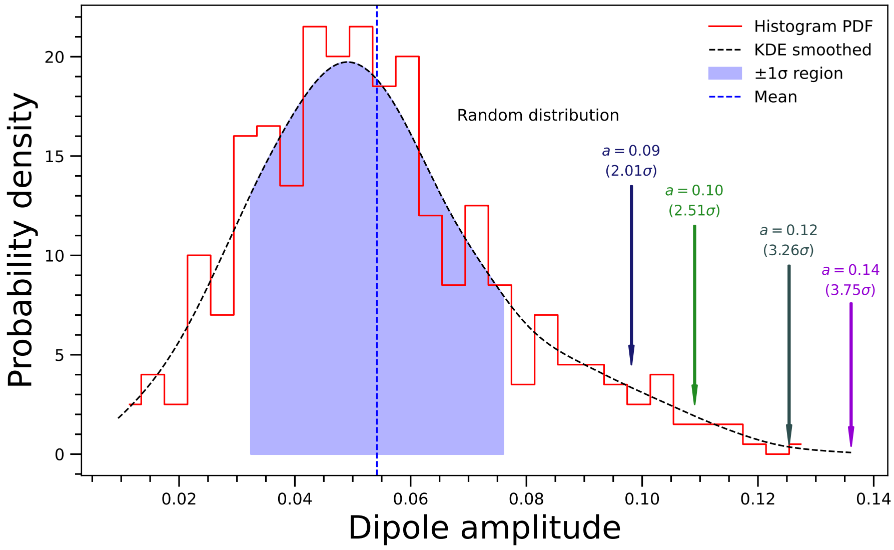

Figure 3: Comparison of dipole amplitudes from four simulated dipole skies ($a = 0.09, 0.10, 0.12, 0.14$) with the estimated PDF obtained from 500 Monte Carlo simulations of isotropic skies (2702 GRBs each). All injected dipole amplitudes lie beyond the 1σ region of the null distribution. The HEALPix resolution parameter $\mathrm{N_{side}} = 8$ has been used for this analysis.

Sl No.	**a**	p-value	Significance (in σ)
1	0.09	0.0479	2.01
2	0.10	0.0193	2.51
3	0.12	0.0024	3.26
4	0.14	0.0003	3.75

Table 1: Statistical significance of the recovered dipole amplitudes for simulated skies with various injected dipole strengths a. All p-values fall below $\alpha = 0.05$.

The results confirm that our method reliably detects dipole anisotropy across a range of amplitudes. For all four cases, the observed dipole amplitudes lie well outside the region expected from random fluctuations under the null hypothesis. Even the lowest injected amplitude of $a = 0.09$ yields a significance level above 2σ, while $a = 0.14$ is detected at nearly 3.8σ. This demonstrates that our framework is sensitive enough to identify dipole signals of modest strength and can robustly distinguish them from statistical noise.

We further examined the detection efficiency of our method by extending the analysis to larger simulated datasets. Specifically, we generated both isotropic and dipole-modulated skies, each containing 20000 points, and compared their dipole amplitudes to assess how sample size influences sensitivity. Following the same procedure as before, we constructed the dipole amplitude distribution from 500 isotropic realizations and compared it against four dipole-injected skies with amplitudes $a = 0.022$, 0.032, 0.042, and 0.052, oriented in the same direction as in the previous test. The corresponding probability distributions and significance levels are shown in Figure 4 and summarized in Table 2.

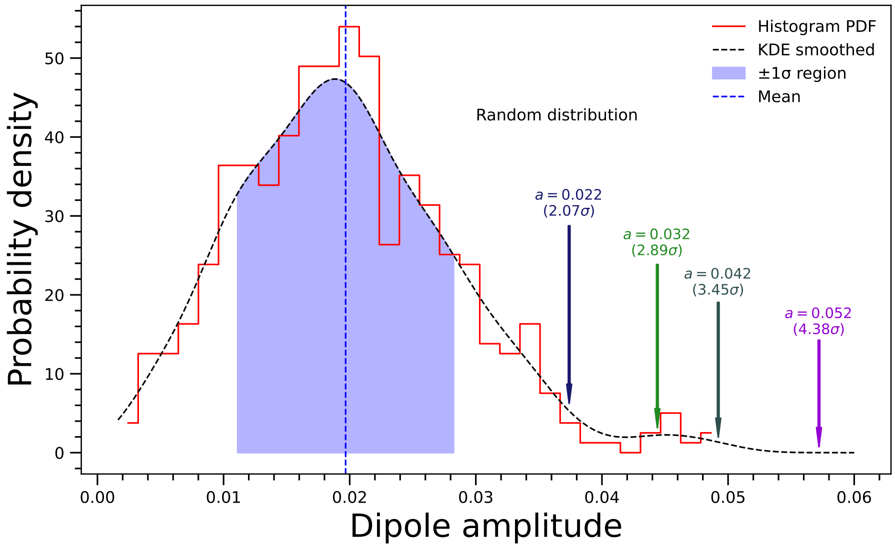

Figure 4: Same as Figure 3, but for simulated isotropic and dipole skies each containing $20{,}000$ points. Four dipole skies with amplitudes $a = 0.022, 0.032, 0.042$, and 0.052 were generated, maintaining the same dipole direction used in Figure 3.

Sl no.	$\mathbf{a}$	p-value	Significance (in σ)
1	0.022	0.0312	2.07
2	0.032	0.0125	2.89
3	0.042	0.0030	3.45
4	0.052	2.387×10^{-6}	4.38

Table 2: Same as Table 1, but for simulations containing 20000 points.

The results clearly demonstrate that increasing the number of data points enhances the sensitivity of the analysis. In this higher-resolution test, even a weak dipole signal with amplitude $a = 0.022$ lies beyond the 2σ region of the isotropic distribution, confirming that the method can reliably detect subtle anisotropies when applied to sufficiently large datasets. This underscores that the efficiency of dipole detection depends not only on the signal strength but also on the statistical size of the sample representing the GRB sky.

3 Results

3.1 Dipole amplitude analysis of BATSE dataset

To assess the statistical isotropy of the BATSE GRB sky, we calculated the dipole amplitude of the observed distribution and compared it with a reference distribution constructed from 500 Monte Carlo realizations of isotropic skies, each containing 2702 GRBs equal to the number in the actual BATSE dataset.

Figure 5 presents the resulting PDF of dipole amplitudes derived from the simulated isotropic skies. The red step histogram represents the binned distribution of dipole amplitudes across these simulations, while the dashed black curve shows the kernel density estimation (KDE), which provides a smoothed representation of the underlying PDF. The shaded blue region indicates the 1σ interval around the mean of the distribution.

The observed dipole amplitude from the BATSE sky is indicated by the vertical blue dashed line and a downward-pointing arrow labeled “BATSE dipole (0.61σ)”. As evident from the figure, the observed value lies well within the 1σ range of the null distribution. This placement suggests that the dipole amplitude measured from the BATSE dataset is consistent with expectations from random statistical fluctuations in an isotropic sky.

The associated p-value, calculated as the probability of obtaining a dipole amplitude equal to or greater than the observed value under the null hypothesis, exceeds the significance threshold of $\alpha = 0.05$. Therefore, we do not reject the null hypothesis of isotropy. In other words, the analysis reveals no statistically significant evidence of large-scale dipole anisotropy in the BATSE GRB distribution.

3.2 Dipole amplitude analysis of Fermi GBM dataset

We perform a similar dipole amplitude analysis for the Fermi GBM dataset, which includes 4032 GRBs detected between 2008 and 2025. As with the BATSE analysis, we compare the dipole amplitude calculated from the observed sky distribution with a null distribution constructed from 500 isotropic Monte Carlo realizations, each containing the same number of GRBs as the Fermi sample.

Figure 6 illustrates the distribution of dipole amplitudes derived from the isotropic simulations. The red step histogram represents the binned PDF, while the black dashed curve shows the kernel density estimate (KDE), providing a smooth approximation of the underlying distribution. The shaded blue region marks the $\pm 1\sigma$ interval around the mean of the null distribution.

The dipole amplitude computed from the Fermi GBM data is shown by the downward-pointing black arrow, labeled “FERMI GBM dipole (-0.44σ)”. Notably, the observed value lies well within the 1σ range of the null distribution, and in fact falls slightly below the mean value derived from the simulations.

This result is consistent with expectations from an isotropic sky and suggests no statistically significant anisotropy in the angular distribution of Fermi-detected GRBs. The associated p-value is well above the significance threshold of $\alpha = 0.05$, leading us to retain the null hypothesis. In other words, the dipole amplitude observed in the Fermi dataset is entirely consistent with random statistical fluctuations expected under isotropy.

3.3 Quadrupole amplitude analysis of the BATSE dataset

To further probe possible anisotropic features in the angular distribution of GRBs, we extended our analysis beyond the dipole term to include the quadrupole component. The quadrupole moment, sensitive to

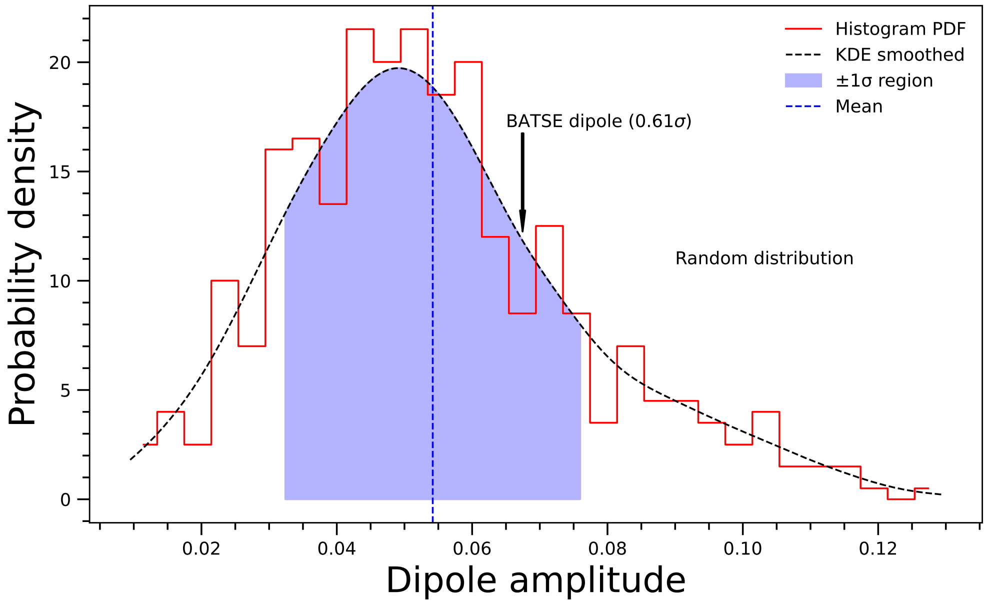

Figure 5: This shows the comparison of the observed dipole amplitude for the BATSE dataset with the PDF obtained from Monte Carlo simulations of 500 isotropic skies containing 2702 points each. The red step histogram shows the binned PDF, while the dashed black line represents the KDE-smoothed curve. The shaded region marks the $\pm 1\sigma$ interval around the mean. The vertical dashed blue line represents the mean of the distribution and the downward black arrow indicates the observed BATSE dipole amplitude, which lies within the 1σ range, suggesting no significant deviation from isotropy. The analysis was performed using a HEALPix resolution parameter of $\mathrm{N_{side}} = 8$.

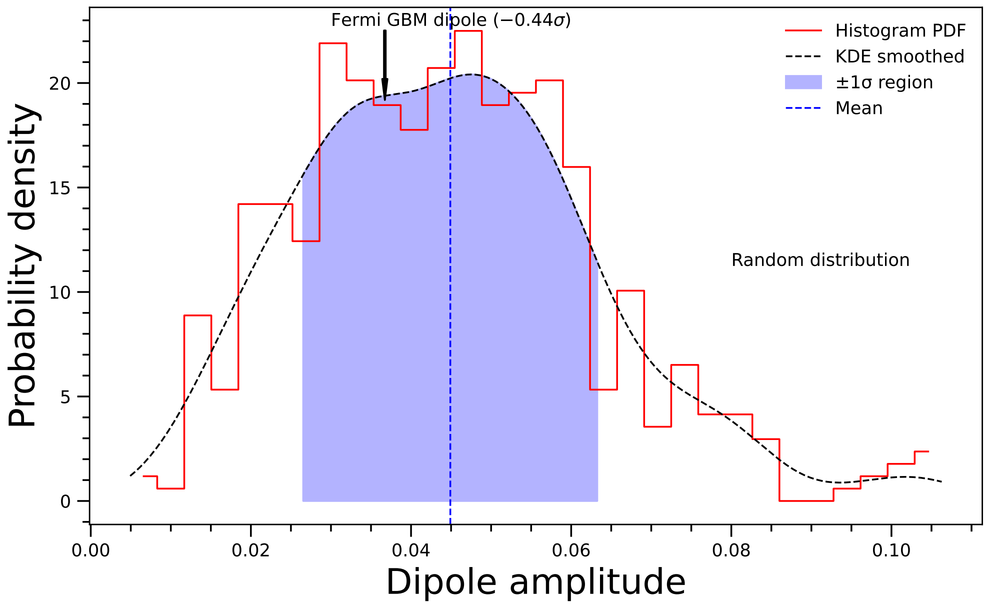

Figure 6: Same as Figure 5 but for Fermi GBM dataset.

planar or axial anisotropies in the sky distribution, was computed using the `anafast` routine of `Healpy`, which estimates the angular power spectrum coefficients C_ℓ from HEALPix maps. In this context, the quadrupole power C_2 represents the variance of the sky distribution at multipole order $\ell = 2$, and its square root provides a convenient measure of the quadrupole amplitude.

Following the same Monte Carlo approach described previously, we generated 500 isotropic skies containing the same number of points as in the BATSE catalog (2702 GRBs). The quadrupole amplitudes of these simulated skies were used to construct a PDF, against which the quadrupole amplitude of the real BATSE sky was compared. The resulting comparison is shown in Figure 7.

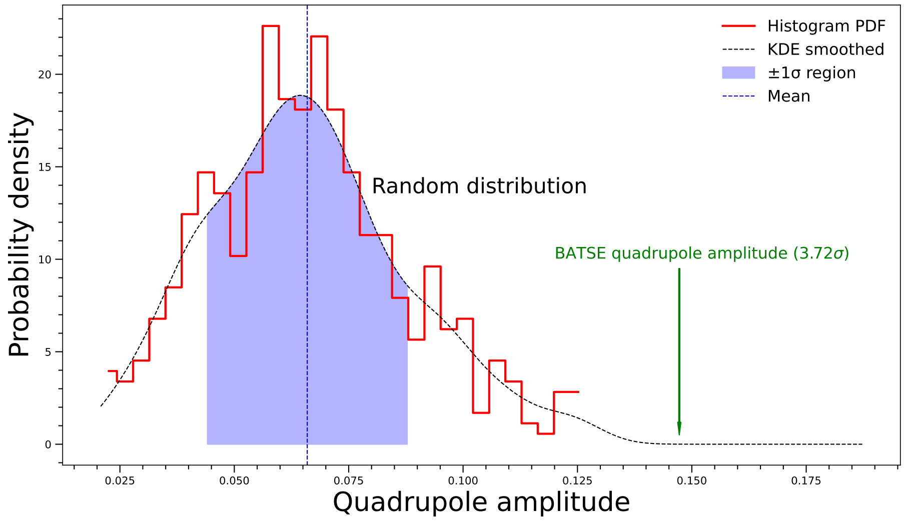

Figure 7: Comparison of the observed quadrupole amplitude for the BATSE dataset (vertical downward arrow) with the PDF constructed from Monte Carlo simulations of 500 isotropic skies, each containing 2702 points. The observed quadrupole amplitude lies approximately 3.72σ above the mean of the isotropic distribution, corresponding to a p-value of 4.306×10^{-6}. The analysis was performed using $\mathrm{N_{side}} = 8$.

The results indicate that the observed quadrupole amplitude in the BATSE GRB distribution is significantly higher than expected from random isotropic realizations. The deviation, corresponding to a statistical significance of approximately 3.7σ, suggests the presence of a weak but non-negligible large-scale anisotropy. While this finding is intriguing, it should be interpreted cautiously, as residual instrumental effects, exposure non-uniformities, or catalog selection biases could potentially contribute to the observed excess. Nevertheless, the result warrants further investigation using independent datasets and higher-resolution analyses to assess the persistence and physical origin of this quadrupole feature.

3.4 Quadrupole amplitude analysis of the FERMI dataset

To complement the quadrupole analysis performed on the BATSE catalog, we extended the investigation to the Fermi GBM GRB dataset, which provides a larger and more recent sample of bursts with improved all-sky coverage. Using the same methodology, we employed the `anafast` routine of `Healpy` to compute the quadrupole power, C_2, from the HEALPix map representation of the Fermi GRB sky. The square root of C_2 was taken as a measure of the quadrupole amplitude, providing a direct assessment of any large-scale planar or axial anisotropies present in the GRB distribution.

A set of 500 Monte Carlo realizations of isotropic skies, each containing 4032 points (matching the size of the Fermi sample), was generated to establish the null distribution of quadrupole amplitudes. The resulting PDF of the simulated quadrupole amplitudes was compared with the measured value from the real Fermi data, as shown in Figure 8.

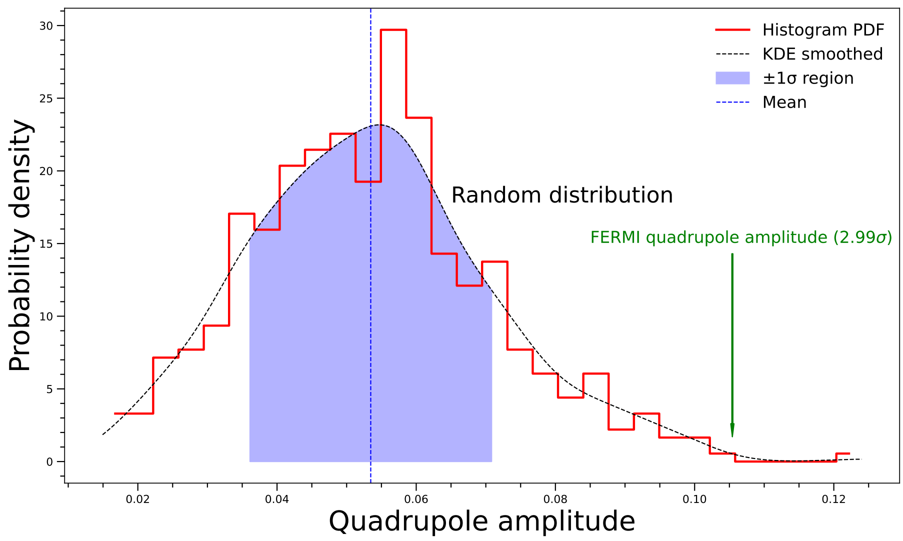

Figure 8: Same as Figure 7 but for Fermi GBM dataset.

The Fermi GBM results reveal a quadrupole amplitude moderately higher than the expectation from purely isotropic skies, with a significance level of about 3σ. This deviation, though less pronounced than that found in the BATSE data, still suggests the presence of a weak large-scale anisotropy in the GRB distribution. The consistency of a non-zero quadrupole signal across two independent GRB datasets, spanning different observational periods and instrumental configurations, may hint at a genuine cosmological origin rather than an observational artifact. However, given that both instruments have different sky exposure patterns and systematic limitations, further analysis particularly with future, uniformly sampled GRB catalogs will be essential to confirm the persistence and nature of this quadrupole signature.

3.5 Testing the significance of the dipole and quadrupole after applying exposure correction to the BATSE dataset

To assess whether the observed large-scale anisotropies in the BATSE Gamma-Ray Burst (GRB) distribution arise from intrinsic cosmic effects or instrumental biases, we performed a detailed analysis incorporating exposure corrections. The sky exposure of the BATSE detector onboard the Compton Gamma Ray Observatory (CGRO) was not uniform, varying primarily with declination due to the spacecraft's orbit and observing constraints. Such exposure non-uniformity can artificially imprint large-scale anisotropies particularly in the dipole and quadrupole moments on the observed GRB sky distribution. To quantify this effect, we employed the BATSE 5B exposure function (Hakkila et al. 2003), which describes the exposure as a function of declination and remains independent of right ascension (RA). Consequently, all subsequent analyses were performed in equatorial coordinates, where this dependence is naturally represented.

We generated mock isotropic skies convolved with the BATSE exposure map to serve as a reference for statistical comparison. The procedure is outlined as follows. The full sky was pixelized using the

HEALPix scheme with a resolution parameter $\mathrm{N_{side}} = 8$, resulting in $12 \times \mathrm{N_{side}}^2$ pixels. The declination value for each pixel was determined using $\mathrm{Dec} = 90° - \theta$, where θ is the polar angle. Exposure values were then assigned to each pixel through linear interpolation of the BATSE 5B exposure data, producing a complete HEALPix map of the exposure function (Figure 9 and Figure 10). These exposure values were normalized to form a probability map, ensuring that the integrated probability across the entire sky equals unity.

Uniformly distributed (θ, ϕ) points were subsequently generated on the celestial sphere. For each point, a random number u was drawn from a uniform distribution between 0 and the maximum exposure probability. A point was accepted if u was less than the corresponding exposure probability value, thereby ensuring that the generated GRB positions follow the BATSE exposure pattern. This procedure was repeated until 2702 GRBs (matching the size of the observed BATSE catalog) were produced for each of the 500 mock skies. Representative examples of these exposure-convolved isotropic skies are shown in Figure 11.

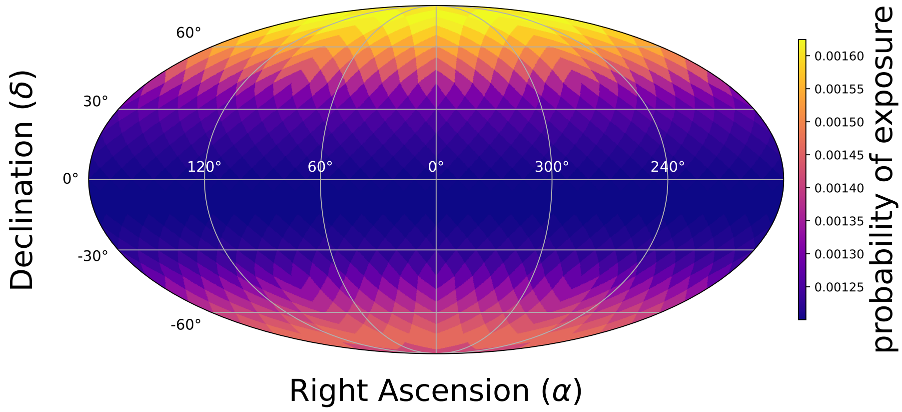

Figure 9: HEALPix probability map of BATSE sky exposure in equatorial coordinates using $\mathrm{N_{side}} = 8$.

We compared the dipole and quadrupole amplitudes of the real BATSE sky with the corresponding PDFs derived from the 500 exposure-convolved isotropic simulations. The dipole results are presented in Figure 12. Once the exposure correction was applied, the apparent dipole signal vanished. The observed dipole amplitude now lies only -0.09σ away from the mean of the isotropic distribution. This demonstrates that the previously detected dipole anisotropy in the uncorrected BATSE data was predominantly driven by the non-uniform sky exposure, rather than by an intrinsic cosmological dipole.

A similar trend is observed for the quadrupole moment. Using the `anafast` routine of `Healpy`, we computed the quadrupole power (C_2) from both the real and simulated exposure-corrected skies, and its square root was taken as the measure of the quadrupole amplitude. The comparison, shown in Figure 13, reveals that the observed quadrupole amplitude is only 0.28σ away from the mean of the exposure-convolved isotropic distribution, corresponding to a p-value of 0.393. Hence, no statistically significant quadrupole anisotropy remains once the exposure correction is applied.

These results jointly demonstrate that both the dipole and quadrupole anisotropies reported in the uncorrected BATSE GRB maps are artifacts of the instrument's non-uniform exposure. Once this effect is rigorously modeled and incorporated into the isotropic simulations, the BATSE GRB sky becomes fully consistent with statistical isotropy. This emphasizes the crucial role of accounting for instrumental systematics in any large-scale anisotropy analysis based on GRB datasets.

Although the BATSE dataset allows for a rigorous treatment of instrumental exposure through the availability of its well-characterized 5B exposure function, no equivalent full-sky exposure maps are

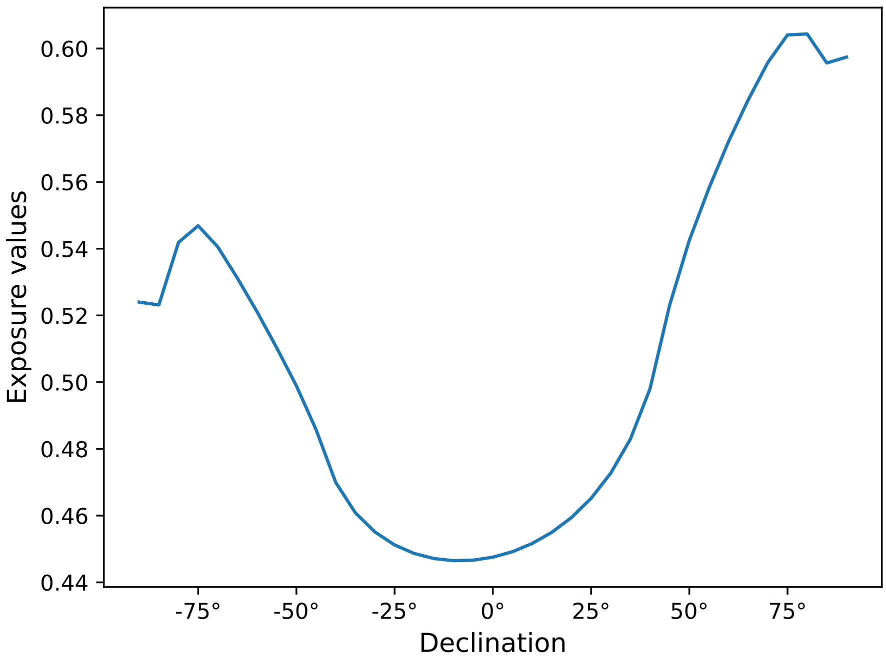

Figure 10: BATSE 5B exposure function as a function of declination. The exposure peaks near the poles and decreases toward the equatorial regions, reflecting the instrument's observing geometry.

publicly available for the Fermi GBM instrument. Consequently, we were unable to perform a similar exposure-corrected isotropy analysis for the Fermi GRB dataset. This limitation is primarily due to the complex observational geometry of Fermi's sky coverage, which varies with both time and energy threshold as the satellite operates in an all-sky survey mode. Nevertheless, the results obtained from the BATSE analysis provide a strong indication of the likely origin of the apparent anisotropies seen in the Fermi data. Given that the Fermi GBM exhibits a non-uniform sky exposure pattern driven by its orbital constraints, Earth occultation, and South Atlantic Anomaly passages, it is reasonable to expect that the observed 3σ quadrupole signal in the Fermi GRB distribution may also arise from residual exposure-related systematics rather than a genuine cosmological anisotropy. A proper exposure correction would likely reduce or even eliminate this apparent excess, as seen for the BATSE case. Therefore, while the Fermi results remain intriguing, they should be interpreted with caution until a detailed, exposure-weighted isotropy test becomes feasible with future data releases or reconstructed exposure models.

4 Conclusions

In this work, we performed a detailed statistical investigation of the angular isotropy of gamma-ray bursts (GRBs) using two of the most comprehensive and widely studied GRB catalogs to date: BATSE and Fermi GBM. Employing a statistical framework built on the HEALPix formalism, we quantified the large-scale angular distribution of GRBs and compared the observed dipole and quadrupole amplitudes with those expected from Monte Carlo realizations of isotropic skies. Our approach, which directly estimates the statistical significance of observed anisotropies by constructing empirical probability density functions, allows for a robust and model-independent assessment of isotropy across the celestial sphere.

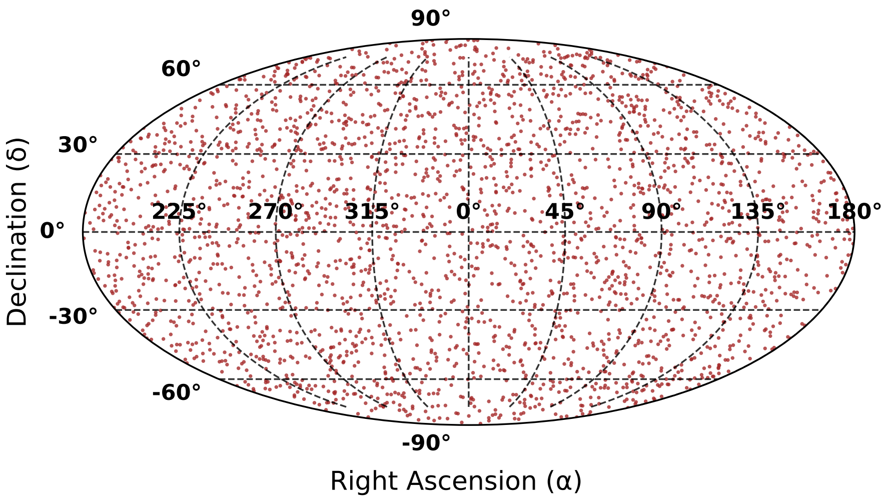

(a) Distribution of GRB positions in a mock exposure-convolved isotropic sky shown in Mollweide projection (equatorial coordinates).

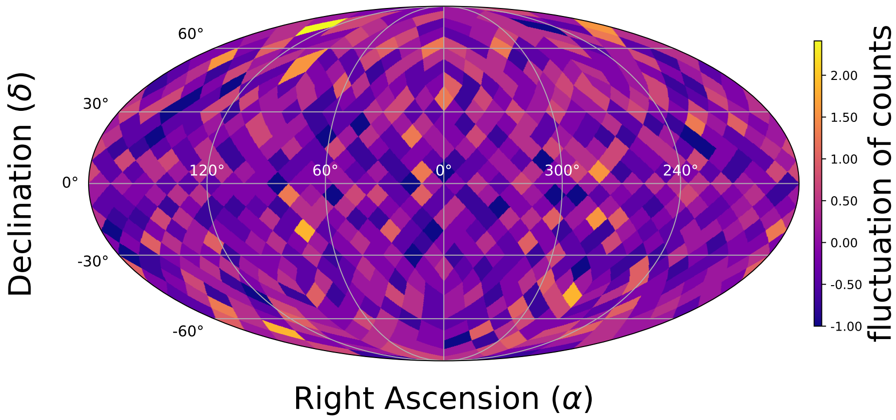

(b) HEALPix map of GRB count fluctuations in a mock exposure-convolved isotropic sky using $\mathrm{N_{side}} = 8$.

Figure 11: Simulated exposure-convolved isotropic skies constructed using the BATSE 5B exposure function. These maps illustrate the modulation of sky uniformity induced by the instrument's varying exposure.

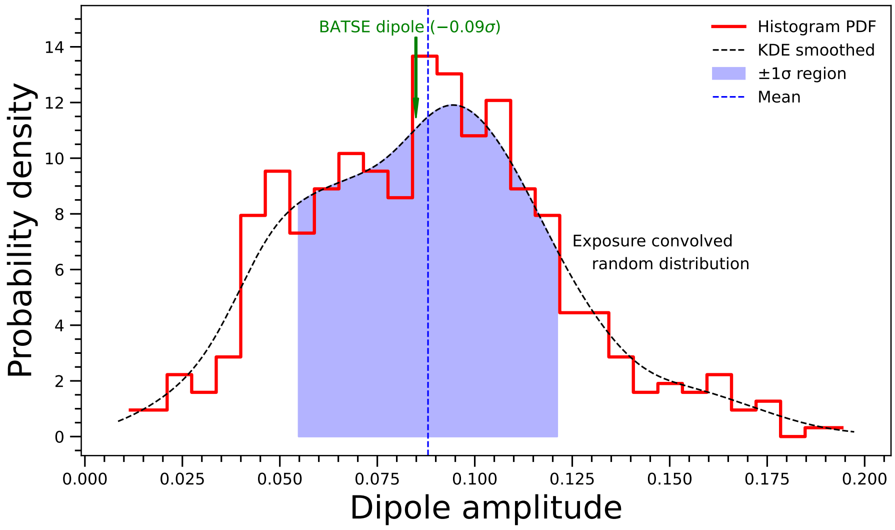

Figure 12: This compares the observed dipole amplitude for BATSE data (vertical downward arrow) with the PDF derived from Monte Carlo simulations of 500 exposure-convolved isotropic skies containing 2702 points each. The observed dipole amplitude lies within 0.1σ of the mean, indicating no statistically significant dipole anisotropy. The HEALPix resolution parameter used is $N_{side} = 8$.

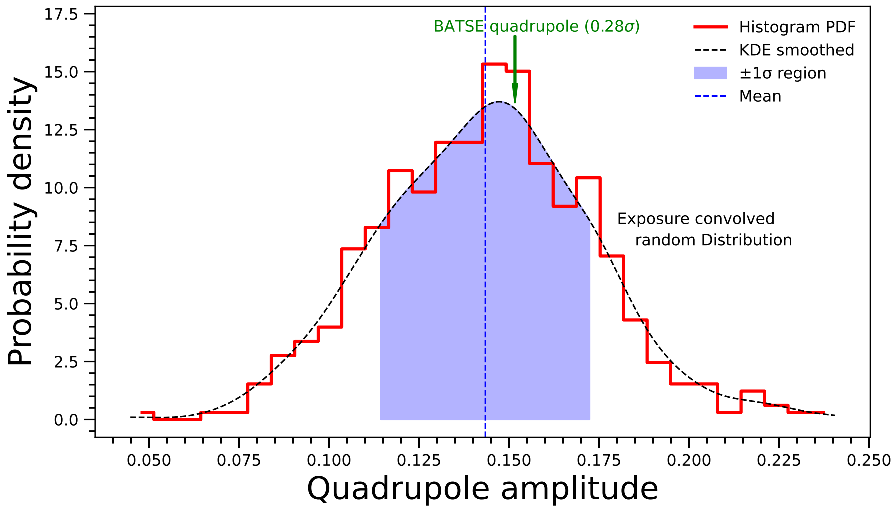

Figure 13: Comparison of the observed quadrupole amplitude for BATSE data (vertical downward arrow) with the estimated PDF obtained from Monte Carlo simulations of 500 exposure-convolved isotropic skies containing 2702 points each. The observed quadrupole amplitude lies 0.28σ away from the mean of the isotropic distribution, indicating no significant deviation from isotropy. The HEALPix resolution parameter used is $N_{side} = 8$.

The analysis of the BATSE dataset, containing 2702 GRBs, reveals no statistically significant dipole anisotropy, with the observed dipole amplitude lying well within the 1σ region of the isotropic distribution. The Fermi GBM dataset, consisting of 4032 GRBs, also shows no evidence of a preferred dipolar direction, supporting the hypothesis of large-scale isotropy in GRB distributions. However, when extending the analysis to the quadrupole term, both datasets exhibit signs of excess power. For BATSE, the quadrupole amplitude initially appears significant at the 3.7σ level, while for Fermi GBM, a milder but still notable 3σ excess is observed.

To investigate the impact of instrumental effects, we further applied exposure corrections to the BATSE data using its publicly available 5B exposure map. After accounting for non-uniform sky exposure, both the dipole and quadrupole signals are found to be statistically consistent with isotropy, suggesting that the earlier quadrupole excess was primarily instrumental in origin. Unfortunately, due to the absence of a publicly available full-sky exposure model for Fermi GBM, a similar correction could not be applied to that dataset. Nevertheless, the analogy with BATSE strongly suggests that the apparent Fermi quadrupole anisotropy is also likely to be an artifact of non-uniform sky exposure rather than a cosmological signal.

The robustness of our methodology was validated through controlled simulations of dipole-injected skies, demonstrating that the framework can reliably detect anisotropies as low as $a = 0.09$ for datasets comparable in size to BATSE. Moreover, tests with larger simulated samples containing 20000 mock GRBs confirmed that the sensitivity improves significantly with increasing sample size, with detectable dipole amplitudes as small as $a = 0.022$. These results establish the reliability and precision of the adopted method for isotropy testing using current and future GRB catalogs. The strengths of our analysis lie in its simplicity, reproducibility, and empirical grounding. By relying on spherical harmonic decomposition and Monte Carlo simulations, we avoid assumptions tied to specific cosmological models or redshift distributions. Moreover, the use of two independent GRB catalogues adds confidence to the null result. However, some caveats remain. Our analysis is limited to angular positions and does not incorporate redshift information, which could offer deeper insight into the evolution of isotropy with cosmic time.

Our findings are in broad agreement with those that report no significant evidence for large-scale anisotropy in GRB distributions (Briggs et al. 1996; Bernui et al. 2008; Řípa and Shafieloo 2019; Andrade et al. 2019). In particular, our results align with works that found long-duration GRBs to be consistent with isotropy, and contribute additional support using an updated, simulation-backed dipole analysis. At the same time, our conclusions contrast with some earlier claims of anisotropy or clustering in GRB datasets (Mészáros 2019; Vavrek et al. 2008; Balázs et al. 1999; Tarnopolski 2017), particularly among short-duration GRBs. These discrepancies highlight the importance of distinguishing between GRB subpopulations and ensuring uniform analysis procedures. Unlike some previous efforts, our method is validated through controlled simulations with known dipole injections, demonstrating its sensitivity to even weak dipole signals.

Overall, our findings reinforce the validity of the cosmological principle on the largest observable scales probed by GRBs. The lack of statistically significant dipole or quadrupole anisotropies once exposure effects are properly accounted for indicates that GRBs trace an isotropic Universe, consistent with the expectations of the standard cosmological model. Future missions with improved sky coverage, uniform exposure, and larger GRB samples will allow for even more stringent tests, potentially revealing subtler deviations that could provide deeper insights into the large-scale structure and evolution of the universe.

5 Acknowledgements

DM thanks Jon Hakkila for sharing the BATSE 5B exposure function. DM would also like to thank P. N. Bhat for useful discussions regarding the FERMI GBM data. BP would like to acknowledge IUCAA, Pune for providing support through associateship programme. AM thanks UGC, Government of India for support through a Junior Research Fellowship.

6 Data availability

The GRB datasets used in this study are publicly avaialble at `https://heasarc.gsfc.nasa.gov/W3Browse/cgro/batsegrb.html` and `https://heasarc.gsfc.nasa.gov/W3Browse/fermi/fermigbrst.html`. Additional data generated and analyzed during this study are available from the authors upon reasonable request.

References

P. k. Aluri, P. Cea, P. Chingangbam, M.-C. Chu, R. G. Clowes, D. Hutsemékers, J. P. Kochappan, A. M. Lopez, L. Liu, N. C. M. Martens, C. J. A. P. Martins, K. Migkas, E. Ó Colgáin, P. Pranav, L. Shamir, A. K. Singal, M. M. Sheikh-Jabbari, J. Wagner, S.-J. Wang, D. L. Wiltshire, S. Yeung, L. Yin, and W. Zhao. Is the observable Universe consistent with the cosmological principle? *Classical and Quantum Gravity*, 40(9):094001, May 2023. doi: 10.1088/1361-6382/acbefc.

U. Andrade, C. A. P. Bengaly, J. S. Alcaniz, and S. Capozziello. Revisiting the statistical isotropy of GRB sky distribution. *MNRAS*, 490(4):4481–4488, Dec. 2019. doi: 10.1093/mnras/stz2754.

S. Appleby, C. Park, P. Pranav, S. E. Hong, H. S. Hwang, J. Kim, and T. Buchert. Minkowski functionals of SDSS-III BOSS: Hints of possible anisotropy in the density field? *The Astrophysical Journal*, 928(2):108, mar 2022. doi: 10.3847/1538-4357/ac562a. URL `https://doi.org/10.3847/1538-4357/ac562a`.

Z. Bagoly, I. Horvath, I. I. Racz, L. G. Balázs, and L. V. Tóth. The Spatial Distribution of Gamma-Ray Bursts with Measured Redshifts from 24 Years of Observation. *Universe*, 8(7):342, June 2022. doi: 10.3390/universe8070342.

L. G. Balázs, A. Mészáros, I. Horváth, and R. Vavrek. An intrinsic anisotropy in the angular distribution of gamma-ray bursts. *Astronomy and Astrophysics Supplement*, 138:417–418, Sept. 1999. doi: 10.1051/aas:1999290.

L. G. Balázs, L. Rejtő, and G. Tusnády. Some statistical remarks on the giant GRB ring. *MNRAS*, 473(3):3169–3179, Jan. 2018. doi: 10.1093/mnras/stx2550.

C. A. P. Bengaly, A. Bernui, I. S. Ferreira, and J. S. Alcaniz. Probing cosmological isotropy with Planck Sunyaev-Zeldovich galaxy clusters. *MNRAS*, 466(3):2799–2804, Apr. 2017. doi: 10.1093/mnras/stw3233.

A. Bernui, I. S. Ferreira, and C. A. Wuensche. On the Large-Scale Angular Distribution of Short Gamma-Ray Bursts. *ApJ*, 673(2):968–971, Feb. 2008. doi: 10.1086/524678.

C. Blake and J. Wall. A velocity dipole in the distribution of radio galaxies. *Nature*, 416(6877):150–152, Mar. 2002. doi: 10.1038/416150a.

M. S. Briggs, W. S. Paciesas, G. N. Pendleton, C. A. Meegan, G. J. Fishman, J. M. Horack, M. N. Brock, C. Kouveliotou, D. H. Hartmann, and J. Hakkila. BATSE Observations of the Large-Scale Isotropy of Gamma-Ray Bursts. *ApJ*, 459:40, Mar. 1996. doi: 10.1086/176867.

R. G. Clowes, K. A. Harris, S. Raghunathan, L. E. Campusano, I. K. Söchting, and M. J. Graham. A structure in the early Universe at z $\sim$ 1.3 that exceeds the homogeneity scale of the R-W concordance cosmology. *Monthly Notices of the Royal Astronomical Society*, 429(4):2910–2916, Mar. 2013. doi: 10.1093/mnras/sts497.

J. Colin, R. Mohayaee, M. Rameez, and S. Sarkar. Evidence for anisotropy of cosmic acceleration. *Astronomy & Astrophysics*, 631:L13, Nov. 2019. doi: 10.1051/0004-6361/201936373.

C. Franco, F. Avila, and A. Bernui. Probing cosmic isotropy in the Local Universe. *MNRAS*, 527(3): 7400–7413, Jan. 2024. doi: 10.1093/mnras/stad3616.

T. Friday, R. G. Clowes, and G. M. Williger. Correlated orientations of the axes of large quasar groups on Gpc scales. *MNRAS*, 511(3):4159–4178, Apr. 2022. doi: 10.1093/mnras/stac269.

C. Gibelyou and D. Huterer. Dipoles in the sky. *MNRAS*, 427(3):1994–2021, Dec. 2012. doi: 10.1111/j.1365-2966.2012.22032.x.

A. Goldstein, J. M. Burgess, R. D. Preece, M. S. Briggs, S. Guiriec, A. J. van der Horst, V. Connaughton, C. A. Wilson-Hodge, W. S. Paciesas, C. A. Meegan, A. von Kienlin, P. N. Bhat, E. Bissaldi, V. Chaplin, R. Diehl, G. J. Fishman, G. Fitzpatrick, S. Foley, M. Gibby, M. Giles, J. Greiner, D. Gruber, R. M. Kippen, C. Kouveliotou, S. McBreen, S. McGlynn, A. Rau, and D. Tierney. The Fermi GBM Gamma-Ray Burst Spectral Catalog: The First Two Years. *ApJS*, 199(1):19, Mar. 2012. doi: 10.1088/0067-0049/199/1/19.

A. Goldstein, R. D. Preece, R. S. Mallozzi, M. S. Briggs, G. J. Fishman, C. Kouveliotou, W. S. Paciesas, and J. M. Burgess. The BATSE 5B Gamma-Ray Burst Spectral Catalog. *ApJS*, 208(2):21, Oct. 2013. doi: 10.1088/0067-0049/208/2/21.

K. M. Górski, E. Hivon, A. J. Banday, B. D. Wandelt, F. K. Hansen, M. Reinecke, and M. Bartelmann. HEALPix: A Framework for High-Resolution Discretization and Fast Analysis of Data Distributed on the Sphere. *ApJ*, 622(2):759–771, Apr. 2005. doi: 10.1086/427976.

D. Gruber, A. Goldstein, V. Weller von Ahlefeld, P. Narayana Bhat, E. Bissaldi, M. S. Briggs, D. Byrne, W. H. Cleveland, V. Connaughton, R. Diehl, G. J. Fishman, G. Fitzpatrick, S. Foley, M. Gibby, M. M. Giles, J. Greiner, S. Guiriec, A. J. van der Horst, A. von Kienlin, C. Kouveliotou, E. Layden, L. Lin, C. A. Meegan, S. McGlynn, W. S. Paciesas, V. Pelassa, R. D. Preece, A. Rau, C. A. Wilson-Hodge, S. Xiong, G. Younes, and H.-F. Yu. The Fermi GBM Gamma-Ray Burst Spectral Catalog: Four Years of Data. *ApJS*, 211(1):12, Mar. 2014. doi: 10.1088/0067-0049/211/1/12.

S. Gupta and T. D. Saini. Direction dependence in supernova data: constraining isotropy. *MNRAS*, 407 (1):651–657, Sept. 2010. doi: 10.1111/j.1365-2966.2010.16945.x.

J. Hakkila, G. N. Pendleton, C. A. Meegan, M. S. Briggs, R. M. Kippen, and R. D. Preece. BATSE 5B Sky Exposure and Trigger Efficiency. In G. R. Ricker and R. K. Vanderspek, editors, *Gamma-Ray Burst and Afterglow Astronomy 2001: A Workshop Celebrating the First Year of the HETE Mission*, volume 662 of *American Institute of Physics Conference Series*, pages 176–178. AIP, Apr. 2003. doi: 10.1063/1.1579333.

M. Haslbauer, I. Banik, and P. Kroupa. The KBC void and Hubble tension contradict ΛCDM on a Gpc scale - Milgromian dynamics as a possible solution. *MNRAS*, 499(2):2845–2883, Dec. 2020. doi: 10.1093/mnras/staa2348.

I. Horvath, Z. Bagoly, L. G. Balazs, J. Hakkila, Z. Horvath, A. P. Joo, S. Pinter, L. V. Tóth, P. Veres, and I. I. Racz. Mapping the Universe with gamma-ray bursts. *MNRAS*, 527(3):7191–7202, Jan. 2024. doi: 10.1093/mnras/stad3669.

R. C. Keenan, A. J. Barger, and L. L. Cowie. EVIDENCE FOR a $\sim$300 MEGAPARSEC SCALE UNDER-DENSITY IN THE LOCAL GALAXY DISTRIBUTION. *The Astrophysical Journal*, 775 (1):62, sep 2013. doi: 10.1088/0004-637x/775/1/62. URL `https://doi.org/10.1088/0004-637x/775/1/62`.

R. Kothari, M. Panwar, G. Singh, P. Tiwari, and P. Jain. A study of dipolar signal in distant Quasars with various observables. *European Physical Journal C*, 84(1):75, Jan. 2024. doi: 10.1140/epjc/s10052-024-12417-1.

C. Kouveliotou, C. A. Meegan, G. J. Fishman, N. P. Bhat, M. S. Briggs, T. M. Koshut, W. S. Paciesas, and G. N. Pendleton. Identification of Two Classes of Gamma-Ray Bursts. *ApJ Letters*, 413:L101, Aug. 1993. doi: 10.1086/186969.

C. A. Meegan, G. J. Fishman, R. B. Wilson, W. S. Paciesas, G. N. Pendleton, J. M. Horack, M. N. Brock, and C. Kouveliotou. Spatial distribution of γ-ray bursts observed by BATSE. *Nature*, 355(6356): 143–145, Jan. 1992. doi: 10.1038/355143a0.

C. A. Meegan, G. N. Pendleton, M. S. Briggs, C. Kouveliotou, T. M. Koshut, J. P. Lestrade, W. S. Paciesas, M. L. McCollough, J. J. Brainerd, J. M. Horack, J. Hakkila, W. Henze, R. D. Preece, R. S. Mallozzi, and G. J. Fishman. The Third BATSE Gamma-Ray Burst Catalog. *ApJS*, 106:65, Sept. 1996. doi: 10.1086/192329.

A. Mészáros. An oppositeness in the cosmology: Distribution of the gamma ray bursts and the cosmological principle. *Astronomische Nachrichten*, 340(7):564–569, Aug. 2019. doi: 10.1002/asna.201913657.

P. Narayana Bhat, C. A. Meegan, A. von Kienlin, W. S. Paciesas, M. S. Briggs, J. M. Burgess, E. Burns, V. Chaplin, W. H. Cleveland, A. C. Collazzi, V. Connaughton, A. M. Diekmann, G. Fitzpatrick, M. H. Gibby, M. M. Giles, A. M. Goldstein, J. Greiner, P. A. Jenke, R. M. Kippen, C. Kouveliotou, B. Mailyan, S. McBreen, V. Pelassa, R. D. Preece, O. J. Roberts, L. S. Sparke, M. Stanbro, P. Veres, C. A. Wilson-Hodge, S. Xiong, G. Younes, H.-F. Yu, and B. Zhang. The Third Fermi GBM Gamma-Ray Burst Catalog: The First Six Years. *ApJS*, 223(2):28, Apr. 2016. doi: 10.3847/0067-0049/223/2/28.

W. S. Paciesas, C. A. Meegan, G. N. Pendleton, M. S. Briggs, C. Kouveliotou, T. M. Koshut, J. P. Lestrade, M. L. McCollough, J. J. Brainerd, J. Hakkila, W. Henze, R. D. Preece, V. Connaughton, R. M. Kippen, R. S. Mallozzi, G. J. Fishman, G. A. Richardson, and M. Sahi. The Fourth BATSE Gamma-Ray Burst Catalog (Revised). *ApJS*, 122(2):465–495, June 1999. doi: 10.1086/313224.

W. S. Paciesas, C. A. Meegan, A. von Kienlin, P. N. Bhat, E. Bissaldi, M. S. Briggs, J. M. Burgess, V. Chaplin, V. Connaughton, R. Diehl, G. J. Fishman, G. Fitzpatrick, S. Foley, M. Gibby, M. Giles, A. Goldstein, J. Greiner, D. Gruber, S. Guiriec, A. J. van der Horst, R. M. Kippen, C. Kouveliotou, G. Lichti, L. Lin, S. McBreen, R. D. Preece, A. Rau, D. Tierney, and C. Wilson-Hodge. The Fermi GBM Gamma-Ray Burst Catalog: The First Two Years. *ApJS*, 199(1):18, Mar. 2012. doi: 10.1088/0067-0049/199/1/18.

B. Pandey. Testing isotropy in the Two Micron All-Sky redshift survey with information entropy. *MNRAS*, 468(2):1953–1961, June 2017. doi: 10.1093/mnras/stx573.

A. A. Penzias and R. W. Wilson. A Measurement of Excess Antenna Temperature at 4080 Mc/s. *ApJ*, 142:419–421, July 1965. doi: 10.1086/148307.

P. Sarkar, B. Pandey, and S. Sarkar. The maximum extent of the filaments and sheets in the cosmic web: an analysis of the SDSS DR17. *MNRAS*, 519(3):3227–3236, Mar. 2023. doi: 10.1093/mnras/stac3722.

S. Sarkar and B. Pandey. Unravelling the cosmic web: an analysis of the Sloan Digital Sky Survey Data Release 14 with the local dimension. *MNRAS*, 485(4):4743–4753, June 2019. doi: 10.1093/mnras/stz499.

S. Sarkar, B. Pandey, and R. Khatri. Testing isotropy in the Universe using photometric and spectroscopic data from the SDSS. *MNRAS*, 483(2):2453–2464, Feb. 2019. doi: 10.1093/mnras/sty3272.

N. Secrest, S. von Hausegger, M. Rameez, R. Mohayaee, and S. Sarkar. A Challenge to the Standard Cosmological Model. *arXiv e-prints*, art. arXiv:2206.05624, June 2022.

N. J. Secrest, S. von Hausegger, M. Rameez, R. Mohayaee, S. Sarkar, and J. Colin. A test of the cosmological principle with quasars. *The Astrophysical Journal Letters*, 908(2):L51, feb 2021. doi: 10.3847/2041-8213/abdd40. URL `https://doi.org/10.3847/2041-8213/abdd40`.

G. F. Smoot, C. L. Bennett, A. Kogut, E. L. Wright, J. Aymon, N. W. Boggess, E. S. Cheng, G. de Amici, S. Gulkis, M. G. Hauser, et al. Structure in the COBE Differential Microwave Radiometer First-Year Maps. *ApJ Letters*, 396:L1, Sept. 1992. doi: 10.1086/186504.

M. Tarnopolski. Testing the anisotropy in the angular distribution of Fermi/GBM gamma-ray bursts. *MNRAS*, 472(4):4819–4831, Dec. 2017. doi: 10.1093/mnras/stx2356.

R. Vavrek, L. G. Balázs, A. Mészáros, I. Horváth, and Z. Bagoly. Testing the randomness in the sky-distribution of gamma-ray bursts. *MNRAS*, 391(4):1741–1748, Dec. 2008. doi: 10.1111/j.1365-2966.2008.13635.x.

A. von Kienlin, C. A. Meegan, W. S. Paciesas, P. N. Bhat, E. Bissaldi, M. S. Briggs, J. M. Burgess, D. Byrne, V. Chaplin, W. Cleveland, V. Connaughton, A. C. Collazzi, G. Fitzpatrick, S. Foley, M. Gibby, M. Giles, A. Goldstein, J. Greiner, D. Gruber, S. Guiriec, A. J. van der Horst, C. Kouveliotou, E. Layden, S. McBreen, S. McGlynn, V. Pelassa, R. D. Preece, A. Rau, D. Tierney, C. A. Wilson-Hodge, S. Xiong, G. Younes, and H.-F. Yu. The Second Fermi GBM Gamma-Ray Burst Catalog: The First Four Years. *ApJS*, 211(1):13, Mar. 2014. doi: 10.1088/0067-0049/211/1/13.

A. von Kienlin, C. A. Meegan, W. S. Paciesas, P. N. Bhat, E. Bissaldi, M. S. Briggs, E. Burns, W. H. Cleveland, M. H. Gibby, M. M. Giles, A. Goldstein, R. Hamburg, C. M. Hui, D. Kocevski, B. Mailyan, C. Malacaria, S. Poolakkil, R. D. Preece, O. J. Roberts, P. Veres, and C. A. Wilson-Hodge. The Fourth Fermi-GBM Gamma-Ray Burst Catalog: A Decade of Data. *ApJ*, 893(1):46, Apr. 2020. doi: 10.3847/1538-4357/ab7a18.

J. Řípa and A. Shafieloo. Update on testing the isotropy of the properties of gamma-ray bursts. *MNRAS*, 486(3):3027–3040, July 2019. doi: 10.1093/mnras/stz921.

A. Wiegand, T. Buchert, and M. Ostermann. Direct Minkowski Functional analysis of large redshift surveys: a new high-speed code tested on the luminous red galaxy Sloan Digital Sky Survey-DR7 catalogue. *Monthly Notices of the Royal Astronomical Society*, 443(1):241–259, 07 2014. ISSN 0035-8711. doi: 10.1093/mnras/stu1118. URL `https://doi.org/10.1093/mnras/stu1118`.

K. K. S. Wu, O. Lahav, and M. J. Rees. The large-scale smoothness of the Universe. *Nature*, 397(6716): 225–230, Jan. 1999. doi: 10.1038/16637.

A. Zonca, L. Singer, D. Lenz, M. Reinecke, C. Rosset, E. Hivon, and K. Gorski. healpy: equal area pixelization and spherical harmonics transforms for data on the sphere in Python. *The Journal of Open Source Software*, 4(35):1298, Mar. 2019. doi: 10.21105/joss.01298.

A Appendix: Stability tests with different HEALPix resolutions

In this Appendix, we examine the stability and robustness of our results against changes in the HEALPix resolution parameter, $N_{\rm side}$. Since the estimation of low-order multipoles such as dipole and quadrupole depends on how the celestial sphere is pixelized, it is important to confirm that our conclusions are not influenced by the chosen resolution. The following analysis tests the consistency of our dipole and quadrupole results for the BATSE dataset when different values of $N_{\rm side}$ are adopted.

A.1 Effects of HEALPix resolution parameter on dipole and quadrupole estimates

The HEALPix resolution parameter $N_{\rm side}$ determines the total number of equal-area pixels on the celestial sphere, given by $N_{\rm pix} = 12 \times N_{\rm side}^2$. A higher $N_{\rm side}$ value provides finer angular sampling but may increase statistical noise for sparse datasets, whereas lower values smooth the map and can slightly affect the estimation of large-scale moments such as dipole and quadrupole amplitudes. Hence, testing the sensitivity of our results to $N_{\rm side}$ provides an important consistency check for the robustness of the analysis.

To evaluate this, we repeated the dipole and quadrupole analyses using exposure-convolved isotropic skies and the BATSE dataset for two higher resolutions, $N_{\rm side} = 32$ and $N_{\rm side} = 64$, in addition to our baseline $N_{\rm side} = 8$. The exposure correction procedure, described in Section 3.5, was consistently applied to all realizations to isolate the effects of pixelization.

Figures 14 and 15 present the resulting PDFs for the dipole amplitudes. At both resolutions, the observed BATSE dipole amplitude lies extremely close to the mean of the isotropic distribution, deviating by only -0.18σ. This confirms that the dipole estimate is highly stable and statistically insignificant across all pixelization scales, reaffirming that the exposure-corrected BATSE sky remains consistent with isotropy.

A similar level of consistency is observed for the quadrupole analysis, as shown in Figures 16 and 17. At $N_{\rm side} = 32$, the quadrupole amplitude differs from the isotropic mean by 0.30σ, while at $N_{\rm side} = 64$ the deviation is 0.27σ. These small deviations confirm that the quadrupole results, like the dipole, are insensitive to the choice of HEALPix resolution.

Overall, this consistency check demonstrates that our conclusions regarding the isotropy of the BATSE GRB sky are robust to variations in the pixelization scale. The observed dipole and quadrupole amplitudes are not artifacts of map resolution, but reflect the intrinsic statistical properties of the data after appropriate exposure correction.

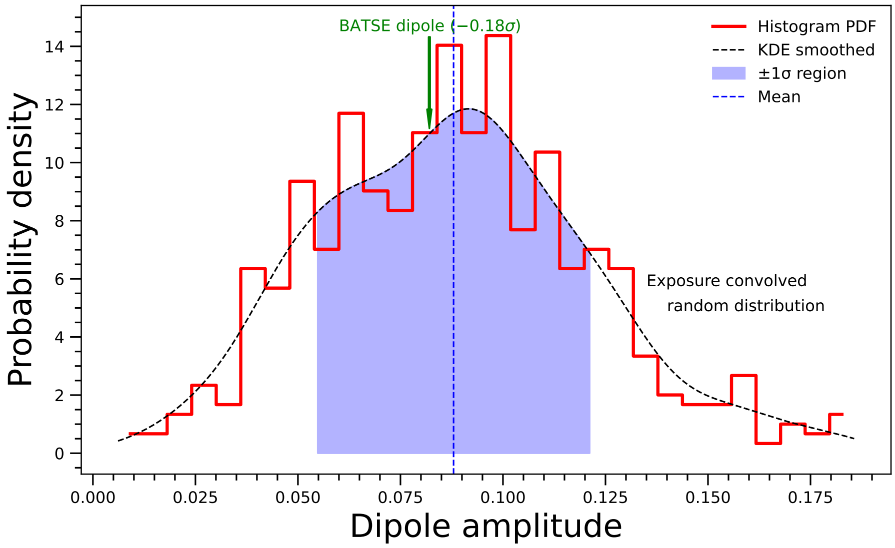

Figure 14: This compares the observed dipole amplitude for BATSE data (vertical downward arrow) with the estimated PDF obtained from Monte Carlo simulations of exposure-convolved isotropic skies containing 2702 points each. The position of the observed dipole amplitude is -0.18σ away from the mean of the isotropic distribution. HEALPix resolution parameter $N_{\rm side} = 32$ has been used.

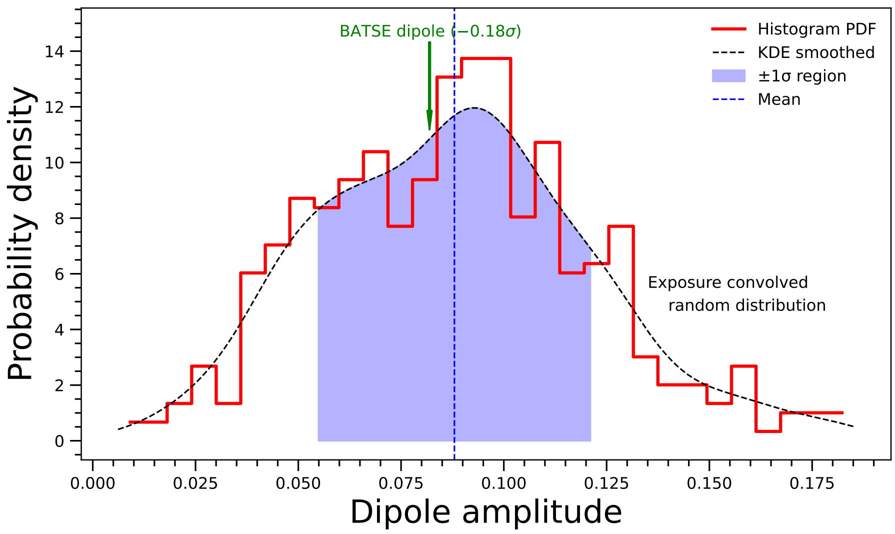

Figure 15: Same as Figure 14, but with HEALPix resolution parameter $N_{\rm side} = 64$. The observed dipole amplitude is -0.18σ away from the mean of the isotropic distribution.

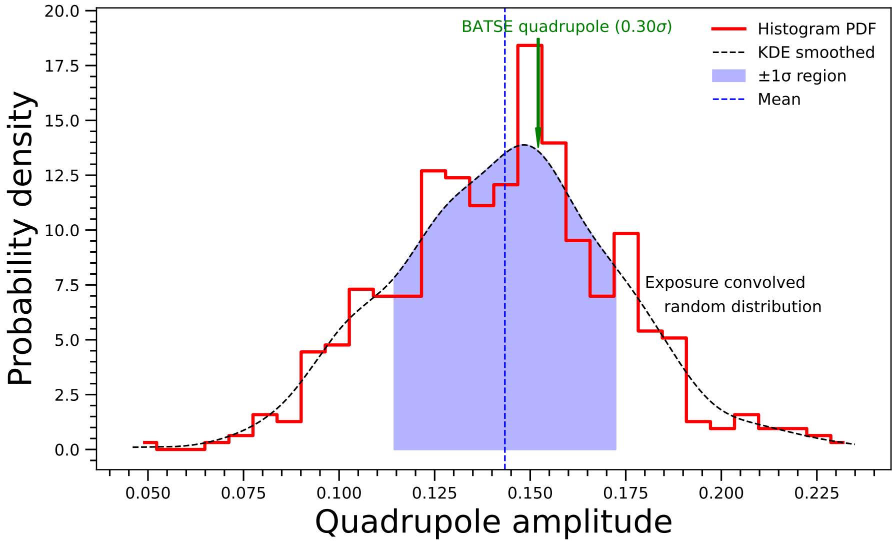

Figure 16: This compares the observed quadrupole amplitude for BATSE data (vertical downward arrow) with the estimated PDF obtained from Monte Carlo simulations of exposure-convolved isotropic skies containing 2702 points each. The position of the observed quadrupole amplitude is 0.30σ away from the mean of the isotropic distribution. HEALPix resolution parameter $N_{\rm side} = 32$ has been used.

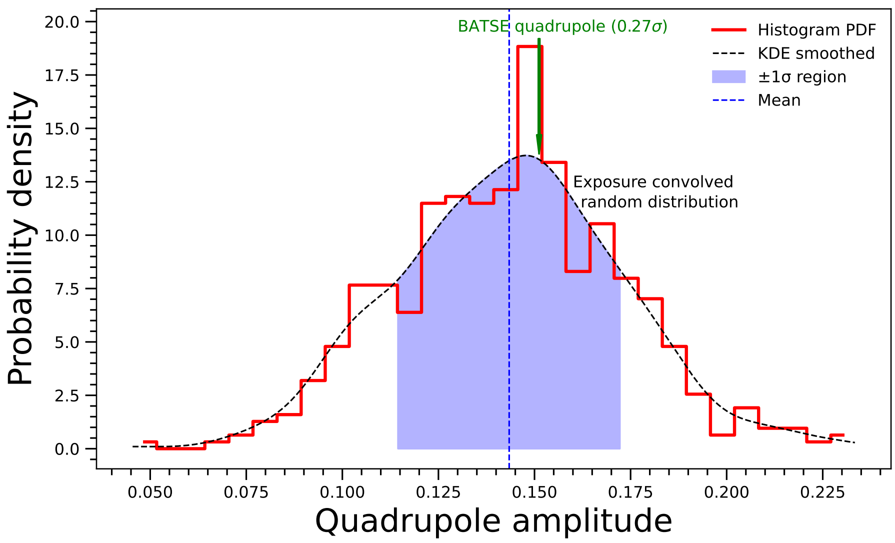

Figure 17: Same as Figure 16, but with HEALPix resolution parameter $N_{\rm side} = 64$. The observed quadrupole amplitude is 0.27σ away from the mean of the isotropic distribution.